Control of Macromolecule Distribution within Synthetic and Biogenic Single Calcite Crystals

J. Aizenberg,[†] J. Hanson,[‡] T. F. Koetzle,[‡] S. Weiner,[†] and L. Addadi*[,†]

Contribution from the Department of Structural Biology, Weizmann Institute of Science, Rehovot 76100, Israel, and Chemistry Department, Brookhaven National Laboratory, Upton, New York 11973

Received August 16, 1996[⊗]

Abstract: The ability of organisms to exercise control over crystal growth is wonderfully exemplified by skeleton formation in echinoderms. A sea urchin spine is a unique composite of a single crystal of calcite and glycoproteins intercalated inside the crystal during its growth. Here we performed a detailed morphological and high-resolution synchrotron X-ray diffraction study of the textures of synthetic and biogenic calcite crystals. We show that the intracrystalline macromolecules from sea urchin spines, when allowed to interact with growing calcite crystals *in vitro*, selectively reduce the coherence lengths and degrees of alignment of the perfect domains in specific crystallographic directions. These directions also correspond to the newly-developed stable faces. In contrast, the defect distribution of young sea urchin spines composed entirely of spongy stereomic structure is much more isotropic. In mature spines containing secondarily filled-in wedges of calcite, the degree of anisotropy is intermediate between that of the synthetic crystals and the young spines. The macromolecules extracted from young and mature spines are, however, very similar. These observations demonstrate the inherent capability of occluded matrix macromolecules to finely differentiate between crystal planes by stereochemical recognition processes. They also show that in biologically-produced calcite crystals this process can be overridden to produce a more isotropic material.

Introduction

Organisms exploit crystals for a variety of purposes, including providing mechanical support and protection for their soft tissues.[1] Surprisingly, a fairly common material-design strategy relies on the use of single calcite crystals as whole skeletal structural units.[2] This requires overcoming the intrinsic brittleness of the crystalline material—a requirement that is achieved, at least in part, by introducing macromolecules inside the crystal in an exquisitely controlled manner.[3]

The macromolecules are occluded inside the single crystal during its formation. Their presence creates defects in the perfect lattice which, in turn, strengthens the crystal against fracture by both absorbing stress and deviating the propagation of cracks along the cleavage planes of calcite.[4] A correlation was also observed between the distribution of the defects and the gross morphology of the biogenic crystals. This suggested a second function of the occluded macromolecules, possibly related to the first, in shaping the biogenic crystals during growth by preferential inhibition of growth in certain directions.[5]

Irrespective of the function, the observed anisotropic distribution of defects implies that the macromolecules are deposited along certain crystal directions rather than others, in a controlled manner.[4,6] It was proposed that the interaction of proteins and glycoproteins with specific crystal planes is governed by intrinsic stereochemical recognition of the macromolecules for specific molecular motifs exposed on certain crystal planes.[7] This concept was supported by *in vitro* experiments of crystal growth in the presence of the macromolecules, which showed morphological modifications of calcite, indicative of selective adsorption of these additives at specific crystallographic surfaces.[3,8] It was recently observed, however, that the morphological and textural symmetry of certain calcitic sponge spicules is lower than that of the calcite structure, suggesting the existence of an additional biological level of control.[9] This would involve targeting of the macromolecules directly to certain surface sites, thus overriding the stereochemical identity of symmetry-related crystal sites.

Here we try to unravel the delicate interplay between "biological" and stereochemical control, addressing two related questions: (i) to unequivocally establish the relation between morphological modification and anisotropic defect distribution in synthetic calcite crystals, grown in the presence of macromolecules extracted from within biogenic crystals; and (ii) to quantitatively compare the extent of anisotropy of the synthetic crystals to that measured in the biogenic crystals, from which the macromolecules were extracted. For this purpose we used young and mature secondary sea urchin spines. Each spine is a single crystal of calcite (of space group $R\bar{3}c$; $a_{hex} = 4.99$ Å,

[†] Weizmann Institute of Science.

[‡] Brookhaven National Laboratory.

[⊗] Abstract published in *Advance ACS Abstracts,* January 15, 1997.

(1) (a) Wainwright, S. A.; Biggs, W. D.; Currey, J. D.; Gosline, J. M. *Mechanical Design in Organisms*; John Wiley & Sons: New York, 1976. (b) Vincent, J. F. V. *Structural Biomaterials*; Macmillan Press: London, 1982. (c) Currey, J. D. In *Skeletal Biomineralization: Patterns, Processes and Evolutionary Trends*; Carter, J. G., Ed.; Van Nostrand Reinhold: New York, 1991; pp 11−26.

(2) Lowenstam, H. A.; Weiner, S. *On Biomineralization*; Oxford University Press: New York, 1989.

(3) (a) Berman, A.; Addadi, L.; Weiner, S. *Nature* **1988**, 331, 546−548. (b) Addadi, L.; Weiner, S. *Angew. Chem.* **1992**, *31*, 153−169.

(4) (a) Berman, A.; Addadi, L.; Kvick, Å.; Leiserowitz, L.; Nelson, M.; Weiner, S. *Science* **1990**, *250*, 664−667. (b) Addadi, L.; Berman, A.; Weiner, S. In *Mechanisms and Phylogeny of Mineralization in Biological Systems*; Suga, S., Nakahara, H., Eds.; Springer-Verlag: Tokyo, 1991; pp 29−33.

(5) Aizenberg, J.; Hanson, J.; Ilan, M.; Leiserowitz, L.; Koetzle, T. F.; Addadi, L.; Weiner, S. *FASEB J.* **1995**, *9*, 262−268.

(6) Berman, A.; Hanson, J.; Leiserowitz, L.; Koetzle, T. F.; Weiner, S.; Addadi, L. *Science* **1993**, *259*, 776−779.

(7) (a) Addadi, L.; Weiner, S. *Proc. Natl. Acad. Sci. USA* **1985**, *82*, 4110−4114. (b) Mann, S. *Nature* **1988**, *332*, 119−124. (c) Mann, S.; Archibald, D. D.; Didymus, J. M.; Douglas, T.; Heywood, B. R.; Meldrum, F. C.; Reeves, N. J. *Science* **1993**, *261*, 1286−1292.

(8) Didymus, J. M.; Oliver, P.; Mann, S.; DeVries, A. L.; Hauschka, P. V.; Westbroek, P. *J. Chem. Soc., Faraday Trans.* **1993**, *89*, 2891−2900.

(9) Aizenberg, J.; Hanson, J.; Koetzle, T. F.; Leiserowitz, L.; Weiner, S.; Addadi, L. *Chem. Eur. J.* **1995**, *7*, 414−422.

S0002-7863(96)02882-X CCC: $14.00

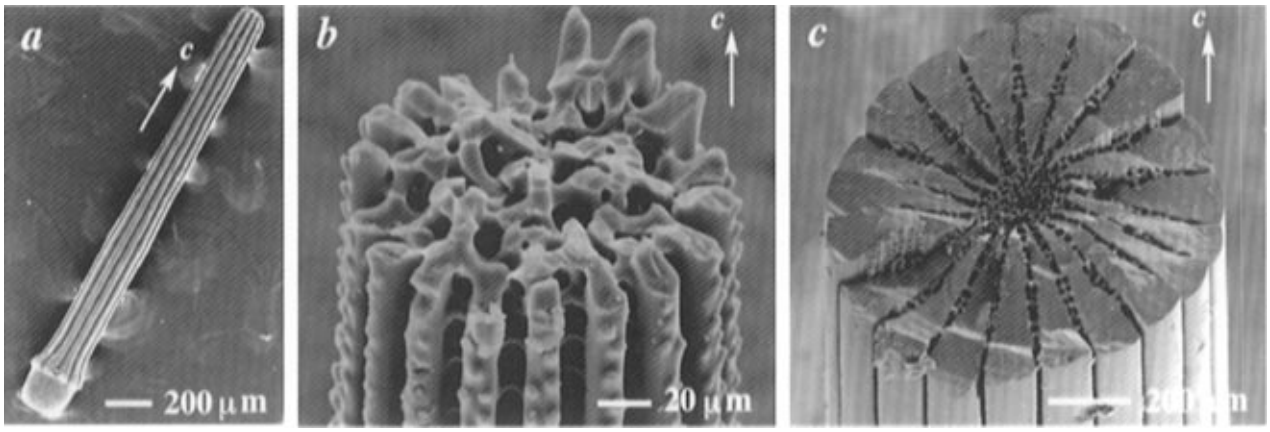

Figure 1. Scanning electron micrographs of secondary spines from the sea urchin *Paracentrotus lividus*. The direction of the *c* axis of the calcite crystal is indicated: (a) intact spine; (b) fracture surface of a young spine, showing the spongy structure of the stereom; (c) fracture surface of the mature spine, showing the development of the sectors that filled the stereom. Note the difference in the sizes of the young and mature spines.

$c_{hex} = 17.06$ Å), with the *c* crystallographic axis along the long axis of the spine (Figure 1a).[10] The newly-formed spines have a convoluted spongy ultrastructure, the stereom, characteristic of almost all echinoderm skeletal elements (Figure 1b).[11] During maturation of the spine, part of the stereom is filled in with more calcite. The resulting mature spines consist of sectors of solid calcite, connected by stereomic junctions (Figure 1c). Each spine still diffracts X-rays as a single crystal of calcite.[10] However, all the fracture surfaces are conchoidal,[12] a behavior reminiscent more of amorphous materials than of calcite with its well-developed cleavage planes.[13]

Berman *et al.* mapped the distribution of defects in a young spine and found a slight anisotropy in the *c* axis direction.[6] This was correlated with the observation that glycoproteins extracted from within the sea urchin skeleton are selectively adsorbed on synthetic calcite crystals along planes roughly parallel to the *c* axis and perpendicular to the *a** axes, of indices {01*l*},[14] and this causes them to develope into stable faces.[3,15] Textural anisotropy could not be detected in the synthetic crystals grown in the presence of spine macromolecules.[16] This was then attributed to the poorly controlled environment of synthetic crystal growth, relative to the biogenic one.

We have now improved our methodology and are capable of detecting anisotropy in these synthetic crystals. We show, in fact, that the anisotropy is larger in the synthetic crystals than in the young sea urchin spines: a counter-intuitive observation reflecting the biological overriding of stereochemical molecular recognition. Futhermore, the extent of anisotropy of the mature spines is intermediate between those of the synthetic crystals and the young spines, suggesting the existence of different mechanisms of control in the two stages of biological crystal growth during spine formation.

Experimental Section

Materials. Spines (young and mature) were separated from the skeletal tests of the echinoid *Paracentrotus lividus* (Mediterranean, Israel) and treated with 2.5% sodium hypochlorite solution on a rocking table for 10 h, in order to remove extraskeletal organic tissue. The specimens were then rinsed several times with double distilled water (DDW) and air-dried. The cleaned secondary spines were arbitrarily subdivided into four groups, ranging from the youngest, completely stereomic spines to the largest mature spines, with pronounced sectors filling most of the stereom. The length/diameter ratio measured for 20 of the youngest and 20 of the most mature spines increases from 10.0 ± 0.9 to 19.2 ± 1.8, respectively.

Crystal Etching. The etch figures on the broken surfaces of the spines from different age groups were obtained by partial dissolution in 0.1 N HCl for 1 min. The specimens were then washed in DDW, dried, mounted on an aluminium stub, sputter coated with gold, and examined in a JEOL 6400 scanning electron microscope (SEM).

Extraction of Intracrystalline Macromolecules. An aliquot of the smallest spines and an aliquot of the largest spines were placed in DDW (10 mg of mineral/100 μL of water) and decalcified by the addition of stoichiometric amounts of 0.01 N HCl, added dropwise over several hours, to avoid drastic changes of pH. The solutions obtained were centrifuged to remove the insoluble material, and the supernatants were exhaustively dialyzed against DDW (Spectrapor 3 dialysis tubing), to yield the total soluble macromolecular extracts. Small aliquots of the two solutions were hydrolyzed in 6 N HCl for 24 h at 110 °C, and their amino acid compositions and concentrations were determined using ninhydrin detection (Dionex BIOLC).

***In vitro* Crystal Growth.** Two types of crystallization experiments were performed. Calcite crystals were epitaxially overgrown on the cleaned spines,[17] and crystals were grown *de novo* in the presence of the intracrystalline macromolecules (1−10 μg/mL). The crystal growth procedures have been detailed previously.[15] Briefly, synthetic calcite crystals were grown for 3 days in a closed desiccator, by slow diffusion of ammonium carbonate vapor into vials containing glass coverslips overlaid by 25 mM calcium chloride solution to which proteins were added as appropriate. The glass coverslips covered with calcite crystals were rinsed with DDW and dried. For detailed morphological analysis of the crystals, one coverslip from each experiment was gold coated and observed in the SEM. The protein contents of the synthetic composite calcite crystals were estimated after dissolving the crystals in 0.1 N HCl. The absolute amounts of calcium and proteins in the

(10) (a) Raup, D. M. In *Physiology of Echinodermata*; Boolootián, R. A., Ed.; John Wiley & Sons, Interscience Publishers: New York, 1966; pp 379−395. (b) Donnay, G.; Pawson, D. L. *Science* **1969**, *166*, 1147−1150.

(11) (a) Dubois, Ph.; Chen, Ch.-P. In *Echinoderm Studies;* Jangoux, M., Lawrence, J. M., Eds.; Balkema: Rotterdam, 1989; pp 109−178. (b) Smith, A. B. In *Skeletal Biomineralization: Patterns, Processes and Evolutionary Trends*; Carter, J. G., Ed.; Van Nostrand Reinhold: New York, 1991; pp 413−444.

(12) (a) Towe, K. M. *Science* **1967**, *157*, 1048−1050. (b) Nissen, H. *Science* **1969**, *166*, 1150−1153.

(13) Lippmann, F. *Sedimentary Carbonate Minerals*; Springer-Verlag: Berlin, 1973.

(14) In hexagonal space groups, the symmetry-related planes in a {*hkl*} set are (*hkl*), (*k*,−(*h*+*k*),*l*), (−(*h*+*k*),*h*,*l*), and their Friedel pairs. Therefore, the {00*l*}, {10$\bar{4}$}, {20$\bar{4}$}, {300}, and {11$\bar{0}$} families examined in this study contain the (006) and (0,0,12$\bar{)}$; (104), (01$\bar{4}$), and (1$\bar{1}$4); (20$\bar{4}$), (024), and (2$\bar{2}$4); (300), (030), and (3$\bar{3}$0); (110), (1$\bar{2}$0), and ($\bar{2}$10) crystallographic planes, respectively. [001], [104], [102], [100], and [110] denote the directions of the diffraction vectors perpendicular to the above-mentioned sets, respectively.

(15) (a) Albeck, S.; Aizenberg, J.; Addadi, L.; Weiner, S. *J. Am. Chem. Soc.* **1993**, *115*, 11691−11697. (b) Albeck, S.; Weiner, S.; Addadi, L. *Chem. Eur. J.* **1996**, *2*, 278−284.

(16) Berman, A.; Hanson, J.; Leiserowitz, L.; Koetzle, T. F.; Weiner, S.; Addadi, L. *J. Phys. Chem.* **1993**, *97*, 5162−5170.

(17) Aizenberg, J.; Albeck, S.; Weiner, S.; Addadi, L. *J. Cryst. Growth* **1994**, *142*, 156−164.

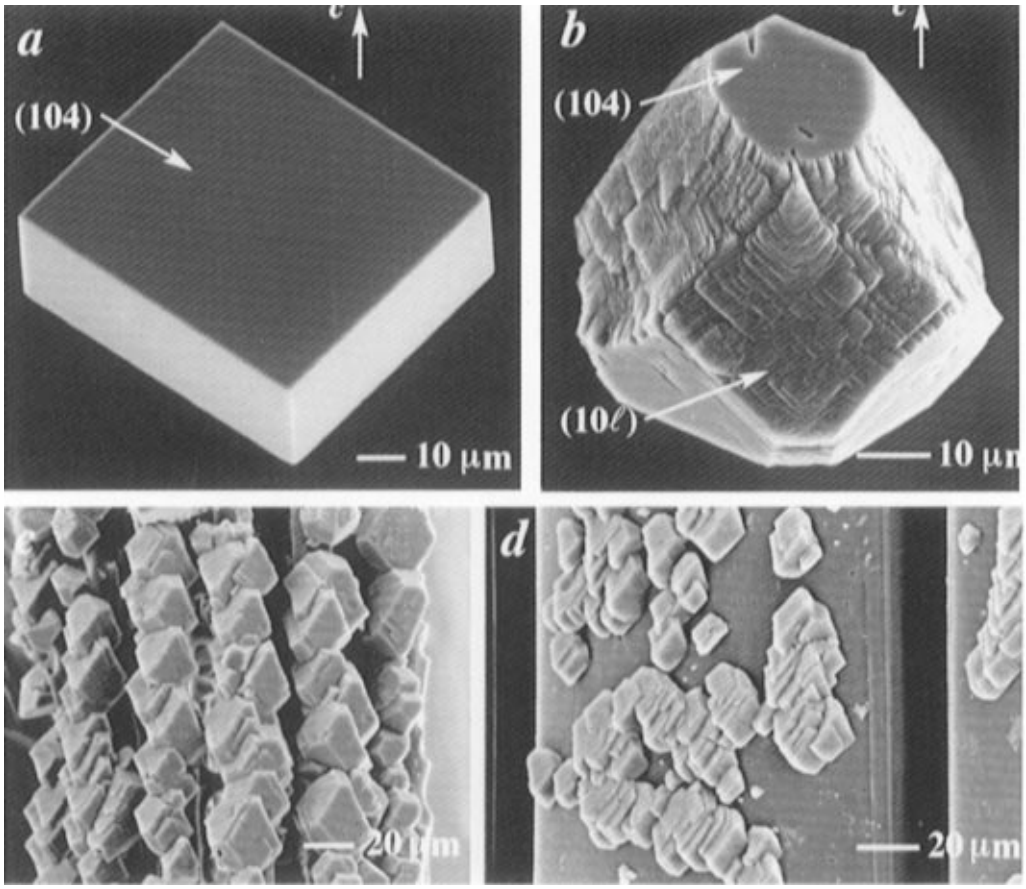

Figure 2. (a) Pure synthetic calcite crystal grown in the absence of additives. Only the stable {104} hexagonal faces are expressed. (b) Synthetic calcite crystal grown in the presence of the macromolecules extracted from *P. lividus* spines. Note the development of a new family of negative rhombohedral faces slightly oblique to the *c* crystallographic axis, indexed as {10*l*} ($l = -1.5$). (c) New calcite crystals overgrown epitaxially on the lateral surface of a young spine. Note that the same faces as in (b) are developed, but the effect of the released macromolecules on the overgrowing crystals is more pronounced and specific. (d) New calcite crystals overgrown epitaxially on the lateral surface of the mature spine. The area corresponds to one sector. The morphological effect is identical to that in (c).

obtained solution were measured using atomic absorption (Perkin Elmer 5100 GFAAS) and quantitative amino acid analysis, respectively.

Synchrotron X-ray Diffraction Measurements of Crystal Textures. As calcite crystals are extremely ordered, measurement of their fine textural parameters is beyond the resolution of standard X-ray equipment. High-resolution diffraction peak profiles of the selected biogenic and synthetic crystals were collected using well-collimated synchrotron X-rays at the National Synchrotron Light Source at Brookhaven National Laboratory (line X7B). The experimental setup has been described previously.[5,6,9] Two parameters of crystal texture were measured.[18] The coherence length (CL) represents the average distance between imperfections in specific crystallographic directions. It can be determined from the width of the diffraction peak in the $\omega/2\theta$ scan mode, by applying the Scherrer formula: $CL = \lambda/(\cos\theta)(B^2_{\omega/2\theta} - \beta^2)^{1/2}]$, where λ is the wavelength, θ is the Bragg angle, and β is the instrumental resolution expressed in radians. In our setup, $\lambda = 0.933$ Å and $\beta = 0.003°$. The peak width, $B_{\omega/2\theta}$ (in radians), was determined from the integrated intensity of the peak in counts per second divided by its maximum intensity after subtracting the background level. The angular spread (AS) characterizes the degree of misalignment between perfectly coherent domains, and is directly deduced from the width of a diffraction peak in the ω scan mode. The following {*hkl*} families of reflections were monitored: {006}, {0,0,12}, {104}, {20$\bar{4}$}, {300}, and {110}.[14] In order to obtain statistically reliable patterns of crystal perfection, three symmetry-related reflections were measured and averaged within each family.

(18) Klug, H. P.; Alexander, L. E. *X-ray Diffraction Procedures*; Wiley-Interscience: New York, 1974.

Results

Synthetic Calcite Crystals with Occluded Macromolecules. Intracrystalline macromolecules were extracted from the youngest and the most mature spines of the sea urchin *Paracentrotus lividus*. The amino acid compositions of the proteins from the two groups are similar, but not identical (Table 1). Significantly, the protein content of the young spines is three times larger (weight % of mineral) than those of the mature spines.

Calcite crystals were grown *in vitro* from solutions containing different concentrations of macromolecules from the two groups of spines. The macromolecules had the same morphological effect on calcite crystals as observed previously from extracts of mixtures of the spines.[3,15] The crystals formed, in addition to the normal {104} faces of pure calcite (Figure 2a), well-developed stepped faces slightly oblique to the *c* crystallographic axis and perpendicular to the *a** axes, indexed as {10*l*} ($l \approx -1.5$) (Figure 2b). No difference in crystal morphology was observed when proteins from young or mature spines were used. The same morphological effect, but much more specific, was observed by direct overgrowth of new calcite crystals on both young and mature spines (Figure 2c,d).

The maximum effect was reached for crystals grown from solutions containing 8 μg/mL of protein. Quantitative amino acid and atomic absorption analyses showed a protein content of 0.04 wt % in the final crystal/protein composite.

Three crystals grown in an 8 μg/mL solution of proteins from spine mixtures, each displaying a pronounced morphological

Table 1. Amino Acid Compositions[a] of the Total Assemblages of Intracrystalline Macromolecules Extracted from the Entirely Stereomic Young Spines and Mature Spines with the Most Pronounced Filling of the Sectors

amino acid	young spines	mature spines
AsX	15.9	15.5
GlX	13.6	12.7
Ser	6.1	4.4
Thr	5.5	6.5
Gly	22.7	19.4
Ala	9.7	8.0
Val	4.7	3.9
Leu	3.5	3.5
Ile	2.4	1.9
Pro	3.4	10.1
Lys	1.0	1.1
His		
Arg	3.7	5.9
Phe	3.8	3.0
Tyr	0.5	0.6
Cys	3.1	2.4
Met	0.3	1.1
protein content[b]	0.07	0.02

[a] Amino acid compositions are expressed in terms of mol %. [b] Protein contents are expressed in wt % of mineral.

effect, were selected for X-ray diffraction studies with synchrotron radiation. The profiles of a series of diffraction peaks from the families {300}, {20$\bar{4}$}, {104}, {00*l*}, and {110}[14] were measured at very high resolution. Note that the reflections from the first three families all correspond to planes that intersect the *a,b* plane along the same line, i.e. perpendicular to the *a** direction (Figure 3a,b, insert). The {110} and {300} planes are parallel to the *c* axis, and form between them a dihedral angle of 30° (Figure 3c,d, insert).

The deduced coherence lengths (size of the domains of perfect structure in directions perpendicular to the diffracting planes) and angular spreads (misalignment between perfect domains) are shown in Table 2. As noted,[5,9,16] the absolute values of coherence length are dependent on the Bragg angle θ of the reflection and therefore cannot be compared directly. Each reflection was thus normalized to the corresponding values in the control calcite crystal. The introduction of this normalization procedure, and the collection of profiles from all 3 symmetry-related reflections from each crystal plane were improvements introduced here, and not used in previous measurements on synthetic crystals.[6] They substantially increase the precision and reliability of the data. The averaged normalized values for each crystal and for each family of reflections are shown in Figure 3. The crystals show a marked reduction in coherence length in the *a,b* plane, relative to the *c* direction (Figure 3a). Furthermore, there is a significant difference in coherence length within the *a,b* plane, between the directions represented by the {300} and {110} reflections (Figure 3c). This result is consistent with preferential adsorption of protein on the {100} planes relative to {110}, as deduced from the morphological changes. The measured angular spreads (Figure 3b,d) show that the domains are markedly misaligned in all crystallographic directions, but follow the anisotropic pattern of the coherence lengths. The largest spread in angular distribution is observed on the planes parallel to the *c* axis, which is consistent with the presence of macromolecules on these planes.

Sea Urchin Spines. The distribution of defects was studied in four sea urchin spines with increasing proportions of wedges (filled sectors) relative to stereom. The same set of measurements was performed as in the synthetic crystals, and the results are presented in Figure 4. In the *a,b* plane of the young entirely stereomic spine, the average coherence length is isotropic in different crystallographic directions and is slightly reduced relative to that in the *c* direction (Figure 4a,c). The reduction in coherence length in the *a,b* plane, relative to the *c* direction, progressively increases with spine maturation. In the most mature spine with very well developed wedges, it is three times larger than in the young one. In addition, there is also a small increase of the defect density in the [100] direction, relative to [110] (Figure 4c). The angular spreads of the perfect domains are 3−8 times higher than in the pure calcite crystal and are very close to the average value obtained for the affected synthetic crystals (Figure 3 and 4b,d). In the young spine, the angular spreads are isotropic in different crystallographic directions. In the course of maturation, the angular spreads may also show a tendency toward anisotropy (Figure 4b,d), although the observed differences are within experimental error. The

Table 2. Measured Textural Parameters in Different Crystallographic Directions[18] for All Calcite Crystals Examined

	{006}		{0 0 12}		{104}		{20$\bar{4}$}		{300}		{110}	
crystal	CL[a]	AS[b]	CL	AS	CL	AS	CL	AS	CL	AS	CL	AS
pure calcite	407	18.5	158	17.8	484	15.7	259	15.5	194	15.5	369	17.2
					448	16.7	276	16.8	147	13.3	424	14.2
					429	17.8	247	13.8	171	14.9	403	21.1
synthetic crystal 1	333	48.4	135	53.4	252	55.1	124	60.9	70	63.0	190	51.7
					245	63.3	n.d.[c]	n.d.	76	63.1	197	61.5
					262	59.4	n.d.	n.d.	72	55.3	208	55.5
synthetic crystal 2	347	61.6	139	55.0	292	64.8	229	84.2	67	86.9	192	81.2
					252	75.3	n.d.	n.d.	74	78.7	183	94.0
synthetic crystal 3	329	71.5	130	69.7	246	100.9	126	99.8	77	113.4	205	96.4
					259	83.7	111	106.0	69	115.3	189	120.2
					289	106.2	n.d.	n.d.	72	120.8	195	110.1
spine 1[d] (young)	267	144.0	85	161.9	241	141.5	145	131.4	84	131.5	195	165.5
					278	124.3	136	122.3	93	112.9	217	128.6
					n.d.	n.d.	n.d.	n.d.	91	102.1	n.d.	n.d.
spine 2	225	149.1	88	157.8	227	140.1	116	125.8	79	110.2	167	135.5
					n.d.	n.d.	n.d.	n.d.	69	132.0	181	164.8
spine 3	248	151.4	85	134.1	224	142.8	103	130.9	64	129.2	176	154.9
					221	120.3	109	124.0	68	111.5	160	135.7
					195	127.3	n.d.	n.d.	68	130.1	n.d.	n.d.
spine 4 (mature)	200	139.7	78	140.3	177	122.9	94	124.1	51	135.8	127	140.3
					153	135.9	80	131.7	51	123.8	130	147.6
					173	120.7	87	129.4	43	120.7	114	136.1

[a] Coherence length (nm). [b] Angular spread (mdeg). [c] n.d. = not determined. [d] The degree of maturation (sector filling) gradually increases from spine 1 to spine 4.

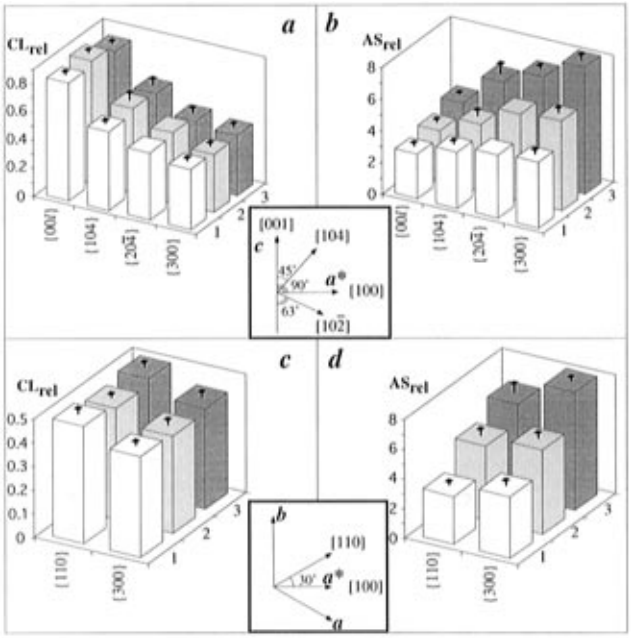

Figure 3. Textural parameters of three synthetic calcite crystals, grown from solutions containing intracrystalline spine macromolecules (8 μg/mL). The data from Table 2 have been normalized to the corresponding values of the control (pure calcite crystal). Each bar represents the average value and the standard deviation for a selected family of crystallographic directions. (a) Normalized coherence lengths in the *c*,*a** planes in directions progressively oblique to the *c* axis. The domain sizes are significantly reduced in the [100] direction relative to [001]. (b) Normalized angular spreads in the *c*,*a** planes in the same directions as in (a). The misalignment of the domains in the [100] direction is significantly larger relative to [001]. Insert for (a,b): Schematic presentation of the diffraction vectors within the *c*,*a** plane, corresponding to the {00*l*} ((006) and (0,0,12)), {104}, {20$\bar{4}$}, and {300} families.[18] (c) Normalized coherence lengths in the *a*,*b* plane. The domain size in the [100] directions is reduced relative to [110]. (d) Normalized angular spreads in the *a*,*b* plane. The misalignment in the [100] direction is significantly larger relative to [110]. Insert for (c,d): Schematic representation of the diffraction vectors for planes (300) and (110) within the *a*,*b* plane.

textural data appear to indicate two different patterns of protein occlusion inside the crystal: one during formation of the stereom and a second during maturation.

Discussion

A clear-cut correlation was established between the morphological modifications induced by adsorption of sea urchin spine macromolecules during growth on synthetic calcite crystals and the distribution of defects inside the grown crystals. Furthermore, the mode of recognition is remarkably specific. The only difference between the manner in which the pure and affected crystals were grown was in the presence of the sea urchin spine macromolecules in solution. This implies that protein adsorption and occlusion caused both the observed morphological modifications and the anisotropic textural changes. This is the first demonstration of the correlation between the two effects, although previous results were explained, based on this tacit assumption. We note, however, that the exact molecular mechanism of defect formation is still unknown. One or more macromolecules may be adsorbed at a given growth site on the crystal, and these may have long-range effects over and above their physically occupied volume. Direct visualization of the occluded macromolecules would be helpful, but is very difficult due to their extremely low concentration within both biogenic and synthetic crystals.

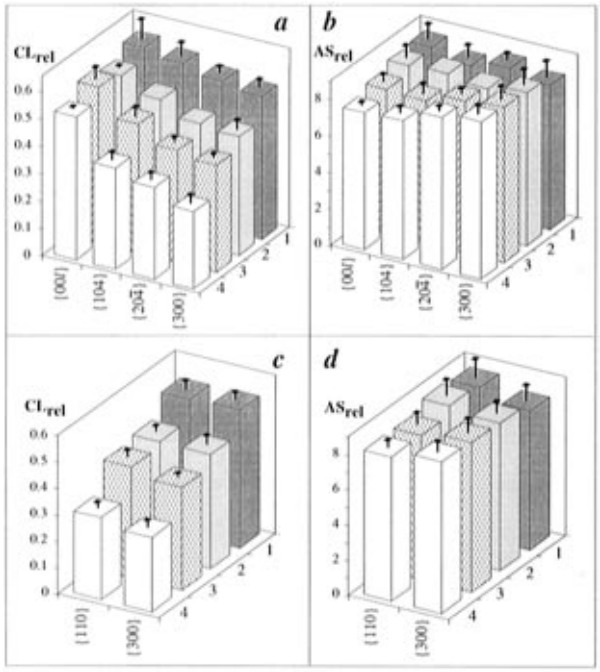

Figure 4. Normalized textural parameters of four sea urchin spines at different stages of maturation (1−4). The presentation is as in Figure 3. (a) Normalized coherence lengths in directions progressively oblique to the *c* axis. In the youngest spine (1), the domain sizes are almost isotropic, while in the most mature spine (4), they decrease significantly from the [001] to [100] direction. (b) Normalized angular spreads in directions progressively oblique to the *c* axis. Only the most mature spine (4) shows a statistically significant increase of the misalignment of the domains. (c) Normalized coherence lengths in the *a*,*b* plane. The domain sizes are reduced in the [100] directions relative to [110] in the most mature spine, whereas they are identical in the youngest spine. (d) Normalized angular spreads in the *a*,*b* plane.

The amino acid compositions of the macromolecules extracted from within young and mature sea urchin spines are similar. They also have the same effect on calcite crystal morphology, inducing the expression of the negative rhombohedral faces {10*l*}, slightly oblique to the *c* axis of calcite and perpendicular to the *a** axes. This indicates similar molecular interactions between macromolecular moieties and selected crystal surfaces. Consistently, increasingly shorter coherence lengths were measured in directions progressively oblique to *c*, with a minimum for [100] (Figure 3). Therefore, intercalation of sea urchin spine macromolecules inside synthetic crystals is very selective on planes parallel to the *c* axis, although a slight reduction in coherence length is observed in the [001] direction as well. Relative to pure calcite crystals, the coherence length is reduced by approximately 15% along [001], and by approximately 60% along [100]. Furthermore, shorter coherence lengths (by about 13%) were measured along [100], relative to [110]. Note that the [100] and [110] directions form between them an angle of only 30°, such that the maximum measurable difference in coherence length is 13%. This is calculated from the projection of the defects on the {110} planes, assuming totally selective adsorption on the {100} planes (CL cos 30° = 0.87CL).

In contrast, the coherence lengths in the young stereomic spines are practically isotropic in different crystallographic directions. Along [001] they are reduced by 40%, and along both the [100] and [110] directions, by 50%, relative to pure synthetic calcite. These results initially appeared to be counterintuitive. It was expected that the biogenic skeletal elements, which crystallize in a very controlled microenvironment, would manifest the highest degree of molecular recognition between

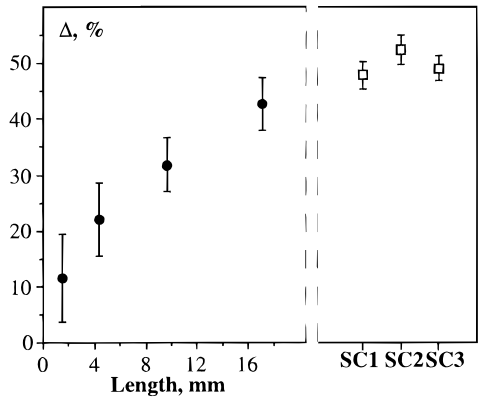

Figure 5. Extent of textural anisotropy (△) of sea urchin spines at different stages of maturation, represented by their different lengths (solid circles), and of synthetic crystals SC1, SC2, SC3 (open squares). △ is defined as follows: , $\triangle(\%) = [(CL_{[001]} - CL_{[100]})/CL_{[001]}] \times 100\%$, where $CL_{[001]}$ and $CL_{[100]}$ are the coherence lengths in the [001] and [100] directions, respectively.

macromolecules and crystal, and the synthetic crystals, grown *in vitro* in the presence of an extracted assemblage of macromolecules, the lowest degree of specificity. The evidence forces us to conclude that the opposite strategy is operative, namely that the cellular activity overrides the intrinsic tendency of the macromolecules to be directed to specific planes. This does not mean that molecular recognition does not exist. The proteins are structured and anisotropic, and so are the crystal surfaces. Their interactions are thus intrinsically non-equivalent on crystallographically different surfaces. This effect, evident in synthetic crystals, is exploited by several organisms and is important in shaping biogenic crystals and altering their mechanical properties.[4,5] This is also confirmed here by the overgrowth experiments. The same macromolecules occluded inside the stereomic spines, released under close to physiological conditions and readsorbed onto newly-formed overgrowing crystals, do manifest their intrinsic recognition capabilities for the selected family of crystallographic planes.

Mature spines with an increasing wedge/stereom ratio are progressively more anisotropic and similar to the synthetic crystals (Figure 5), although their protein content is lower than in the stereom. We conclude that filling of the wedges occurs with a mechanism different from the stereom formation, and more closely resembles crystal growth from solution.

We do not know what advantage this double mechanism may afford the final product. Mechanically, the mature spines including the wedges fracture in a manner similar to the stereomic material, namely with a conchoidal fracture.[12,19] We may, however, speculate about the mechanism by which the stereom forms. The stereom grows into a convoluted labyrinthic structure. At each junction it must expand in many different crystallographic and spatial directions. It is reasonable to assume that the intracrystalline macromolecules are involved in limiting and modulating growth at each stage, and thus need to be secreted and directed to specific sites in a continuous modeling process at the submicron level. The interactions with the growing crystal are thus more isotropic in the stereom than in the wedges. This may also be the reason why the macromolecular content is three times greater in the stereomic material than in the wedge "filling".

The stereom is widely used by echinoderms as a building material in various locations, and is modeled into many different shapes.[11] We propose that this is an "all-purpose" material, designed in such a way as to be adaptable to all desired shapes and mechanical functions. The macromolecules are most probably involved in both the shaping and strengthening processes. Their continuous interference with the growing crystal is well controlled by cellular activity, with the cells releasing them into a very limited microenvironment juxtaposed to the growing surface.[2,20]

Acknowledgment. This study was funded by Grant No. 92−00100 from the US−Israel Binational Science Foundation. The research carried out at Brookhaven National Laboratory was under contract DE-AC02-76CH00016 with the U.S. Department of Energy and supported by its Division of Chemical Sciences, Office of Basic Energy Sciences.

JA9628821

(19) (a) Emlet, R. B. *Biol. Bull.* **1982**, *163*, 264−275. (b) O'Neill, P. L. *Science* **1981**, *213*, 646−647.

(20) (a) Simkiss, K. In *Biomineralization in Lower Plants and Animals*; Leadbeater, B. S. C., Riding, R., Eds.; Clarendon Press: Oxford, 1986; pp 19−37. (b) Simkiss, K.; Wilbur, K. M. *Biomineralization. Cell Biology and Mineral Deposition*; Academic Press: San Diego, 1989. (c) Mann, S. In *Biomineralization. Chemical and Biochemical Perspectives*; Mann, S., Webb, J., Williams, R. J. P., Eds.; VCH Publishers: Weinheim, 1989; pp 189−222.